load values and develop conservative allowable bearing pressures for compacted fill and natural overburden materials.

3. The consideration for inundation of shallow spread footings was addressed in the program with the establishment of noninundated conditions to apply to all footings embedded 4 ft or more below final constructed grade. Inundated conditions apply to all footings embedded less than 4 ft below final constructed grade.

4. The proposed allowable bearing pressures developed from the load test program were higher than the locally accepted values. Providing these allowable bearing pressures as design criteria to the project design consultants is expected to result in more uniformity in foundation design and considerable cost savings to this project.

ACKNOWLEDGMENTS

The authors wish to express their appreciation to Dean Lindsey, I-10 Principal Engineer, Arizona Department of Transportation, and the Federal Highway Administration for authorizing this special load test program. The participation of Ken Ricker, Western Technologies, Inc., in assembly, installation, and operation of the testing equipment is gratefully acknowledged.

REFERENCES

1. H.F. Winterkorn and H-Y. Fang. Foundation Engineering Handbook. Van Nostrand Reinhold Company, New York, 1975, pp. 121-147.
2. D.D. Burmister STP No. 322. Prototype Load-Bearing Tests for Foundations of Structures and Pavements, ASTM, Philadelphia, Pa., 1962.
3. G.A. Leonards. Foundation Engineering. McGraw-Hill Book Company, New York, 1964, pp. 588-594.
4. J.E. Bowles. Foundation Analysis and Design. McGraw-Hill Book Company, New York, 2nd ed., 1977, pp. 95-101, 113-122.

Publication of this paper sponsored by Committee on Foundations of Bridges and Other Structures.

# Prediction of Axial Capacity of Single Piles in Clay Using Effective Stress Analyses

ANDREW G. HEYDINGER and CARL EALY

ABSTRACT

This paper contains a description of research conducted on piles in clay. A finite element program was used to compute the state of stress in the soil around piles. The formulation accounts for the effects of pile installation and soil consolidation, updating the effective stresses continuously in a step-wise manner. The results of an approximate elastic solution were compared with the finite element solution. The two solutions were used to derive expressions for the effective radial stress after consolidation. A predictive procedure was developed that uses the effective radial stress to calculate the side resistance of piles in clay.

Investigators have attempted to determine the state of stress around piles in clay in order to estimate side frictional capacity (1-11). To this end, the state of stress in the soil is updated from the in situ condition to the conditions immediately following pile installation and soil consolidation, and at pile failure. The purpose of this paper is to describe the results of two computer solutions for the effects of pile installation, and to propose a design procedure for axially loaded piles in saturated clays for bridge foundations and other structures.

CAMFE is an acronym for Cambridge finite element, a program developed at the University of Cambridge (12). It uses a one-dimensional finite element formulation to determine the pore pressure and stress changes that occur during pile installation and soil consolidation. For this investigation, an elasto-plastic model was used to represent the soil. The results obtained from CAMFE for the pore pressure and stress changes resulting from installation are similar to those obtained from a cylindrical cavity expansion theory (13) for an elastic, perfectly plastic material. The consolidation phase of the formulation is completed assuming that water flows outward only radially. Thus, as with the cavity expansion procedure, plane stress conditions exist.

The other solution that was used is referred to as VECONS (5). It uses cylindrical cavity expansion theory to model pile installation and and an approximate elastic solution to model consolidation. For the consolidation process, it is assumed that the soil modulus varies from the pile surface to a predetermined distance from the pile. Thus, it is an acronym for Variable-E-Consolidation. The solution--a modification of a solution proposed by others (14)--allows anisotropic soil stiffness to be input for the radial and circumferential stiffnesses to better physically represent the effects of pile installation.

To develop the predictive procedure, comparisons were made between the two analyses. On completion of the comparisons, a parametric study was conducted using the two programs to predict the state of stress in the soil after consolidation for a number of conditions. The results of the analyses are shown as the radial effective stress after consolidation normalized by the undrained shear strength. The radial effective stress after consolidation is then used to predict side capacity using the correlations between radial stress and side capacity (15-16).

## DESCRIPTION OF CAMFE AND VECONS

As already mentioned, CAMFE is a one-dimensional finite element program that uses an elasto-plastic soil model. The elasto-plastic soil model uses a volumetric work-hardening plasticity formulation to represent the soil behavior during yielding. Plastic yielding occurs when the yield criterion is met. The yield criterion, which is referred to as the modified Cam-clay soil model (2), specifies an elliptical yield surface when plotting the deviator stress versus the mean normal stress.

Pile installation is modeled assuming that soil is expanded radially from a finite radius to a larger radius. The authors of the program have shown that the stresses and excess pore pressures after expansion are equivalent to those obtained from cylindrical cavity expansion, when the initial radius is doubled (2). At the end of installation, there is a zone of soil around the pile that has failed in shear, which then reaches a state referred to as the critical state (17). The resulting stresses and excess pore pressure after installation then become the initial conditions for the consolidation process.

Consolidation occurs when the excess pore pressures around the pile dissipate. The assumption that radial consolidation occurs results in conditions in which the radial stress is the maximum principal stress and the vertical and circumferential stresses are the minimum principal stresses. At the end of consolidation, the ratio between the vertical and circumferential stresses and the radial stress is equivalent to the at-rest lateral earth pressure coefficient for normally consolidated soil. Thus, the soil yielding that occurs during installation causes the soil to behave as a normally consolidated soil. After consolidation, the soil is not at the critical state.

VECONS was written for use in modeling pile installation effects (5). Plane strain cylindrical cavity expansion theory is used to determine the pore pressure and stresses immediately after installation. For cylindrical cavity theory, it is assumed that the soil behaves as an elastic, perfectly plastic material. After shearing occurs, it is assumed that the soil reaches and remains at the critical state for further deformations so that the effective stresses remain constant. There is a zone of soil around the pile at the critical state. Soil outside the critical state zone deforms elastically.

An approximate solution proposed by others (14) was modified in order to compute the state of stress in the soil after consolidation. It is assumed that the soil modulus varies logarithmically as a downward-facing parabola from the pile surface to the outside boundary of the critical state zone. A value of the ratio of the radial soil modulus $E_{ri}$ at the pile surface to the radial soil modulus ($E_{ro}$) at the outside boundary equal to 0.1, and a drained Poisson's ratio equal to 0.3 were used. To obtain a set of equations that could be used to solve the stress changes during consolidation, the constitutive equations were substituted into the equation of equilibrium of total stress. The resulting equations were then solved by dividing the yielded zone into a number of subzones and writing the boundary conditions for the boundaries of the subzones.

The major modification to the published solution was the use of an anisotropic formulation for the soil modulus. It was assumed that the soil modulus in the circumferential direction, $E_\theta$, was greater than the modulus in the radial direction, $E_r$ ($E_\theta/E_r$ = 2 was used). This effectively caused the soil to stiffen in the circumferential direction, which then reduced the radial stress changes. Thus, the radial stresses after consolidation, and the inferred side resistance that could be developed, were reduced to values that agreed with measured capacities (5).

The computed states of stress after soil consolidation from VECONS were input into AXIPLN, an axisymmetric finite element program plan (18), which was then used to model pile loading. Good agreement was obtained between measured and computed values of shear stress along the pile and load in the pile for three well-instrumented pile load tests. This verifies that VECONS can be used to predict the state of stress in the soil for at least the zone of soil immediately adjacent to the pile.

## COMPARISONS BETWEEN CAMFE AND VECONS

Comparisons between CAMFE and VECONS for five different soils that have been well documented are given. Information on the first two sites was obtained from the investigators working at Cambridge who developed CAMFE. This includes Boston Blue Clay with overconsolidation ratios (OCR) of 1 and 8 (10) and London Clay with an OCR of 8 (11). The other three soils include Beaumont Clay at the University of Houston test site (19), San Francisco Bay Mud at the Hamilton Air Force Base site (20), and Champlain clay at the St. Alban test site near Quebec, Canada (21,22). The results are shown as plots of stress or pore pressure normalized by the initial undrained shear strength that was obtained from the CAMFE analyses, versus the natural logarithm of the radial distance from the pile surface. Figure 1 shows the results obtained for Boston Blue Clay with an OCR of 1 (10), and Figure 2 shows results obtained for London Clay with an OCR of 8 (11).

A summary of the results of the analyses is given in Tables 1 and 2. Tables 1 and 2 also give the normalized stress changes that occur immediately after pile installation and after consolidation for the CAMFE and the VECONS analyses. The in situ undrained shear strength was used in all cases to normalize the stresses. For both solutions, it was necessary to model the stresses at a radial distance greater than at the pile surface, $r > r_o$. It was determined that representative results could be obtained by using r values of 1.10 $r_o$ for VECONS and 1.15 $r_o$ for the CAMFE analyses. Based on the comparisons, it was determined that the normalized stresses from both analytical models should be used to represent stresses acting on piles.

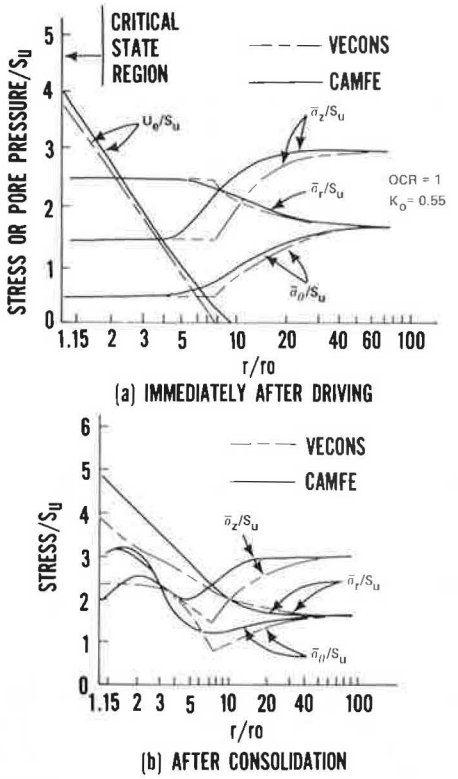


FIGURE 1 Comparison of results of CAMFE and VECONS on Boston Blue Clay (OCR=1) *(10)*.

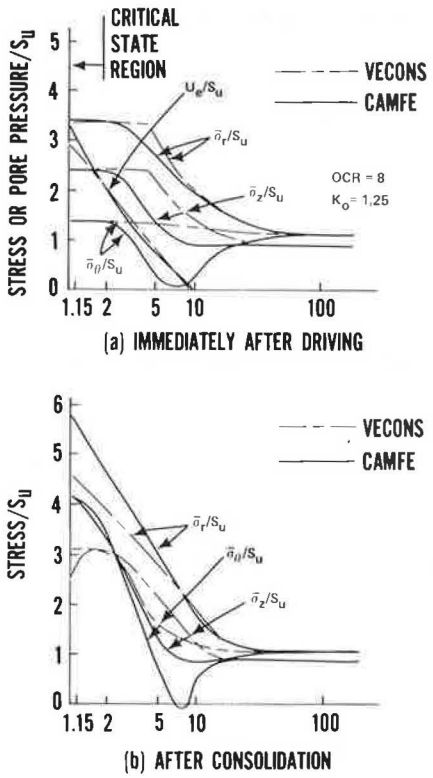


FIGURE 2 Comparison of results of CAMFE and VECONS on London Clay (OCR=8) *(11)*.

Computational difficulties arise when modeling normally or lightly overconsolidated soils with CAMFE. Indications of the difficulties include negative values of the void ratio and the pore pressure, and values of the stresses that are obviously erroneous. In addition, the solution may encounter a step requiring that the square root or logarithm of a negative number be taken. The difficulties can be avoided if large values of $\kappa$ and $\lambda$ (critical state parameters for Cam-clay) that are not repre- sentative of the actual soil conditions are input. Because of the difficulties, CAMFE was only used to model overconsolidated soils in the subsequent analyses.

## PARAMETRIC STUDY OF CAMFE AND VECONS

Parametric studies were conducted to determine dependence of soil properties and stress history on the results obtained from CAMFE and VECONS. Similar studies reported by Wroth et al. (11) indicate that the results from CAMFE depend only on two parameters, M and $\lambda$, where M is a function of the peak effective angle of internal friction [6 sin $\phi'$/(3-sin $\phi'$)], and $\lambda$ is the compression index using a plot of the natural logarithm of the vertical effective stress. The effects of soil stress history were determined for this investigation by characterizing soils with different values of OCR with representative values of $K_o$ and the ratio of the undrained shear strength to the means effective overburden pressure, $s_u/p'_o$.

Conclusions from the parametric study with CAMFE and VECONS are similar to those from the previous study with CAMFE. The normalized effective radial stress is not affected by the effective vertical overburden pressure (depth) and the in situ soil modulus, $E_u$. The final effective radial stress depends on $\phi'$ (equivalent to M for the CAMFE input) and $s_u$. The most significant changes occurred when $\lambda$ and M were varied. The ratio $s_u/p'_o$ has a lesser effect than M and $\lambda$. However, it was utilized in this study to investigate the effects of soil stress history. Because the results of the two solutions are similar, analyses with both CAMFE and VECONS were con conducted by varying M or $\phi'$, $\lambda$ (CAMFE only) and the OCR (as characterized by typical values of $s_u/p'_o$ and $K_o$).

## ANALYSES FOR THE EFFECTS OF PILE INSTALLATION

The results of the analyses were obtained from a parametric study using the CAMFE and VECONS solutions. The objective of the analyses was to determine the effective radial stress after soil consolidation in terms of known soil properties to predict the maximum side resistance along piles in clay. The results are presented in terms of the normalized effective radial stress, $\sigma'_{rc}/s_u$.

A plot of the final radial effective stress normalized by $s_u$ versus M is shown in Figure 3. The curves showing the results of the CAMFE analyses are for values of $s_u/p'_o$ = 0.8 and 1.0 for $\lambda$ = 0.1; and $\lambda$ = 0.3, and $s_u/p'_o$ = 1.2 for $\lambda$ = 0.5. The curves represent the upper ($\lambda$ = 0.1, $s_u/p'_o$ = 0.8) and lower ($\lambda$ = 0.5, $s_u/p'_o$ = 1.2) range of values that occur. Values of $s_u/p'_o$ that are less than 0.8 could not be used because of the computational difficulties previously described. A ratio of $\kappa/\lambda$ = 0.2 was used throughout. The previous analyses indicated that $\sigma'_r/s_u$ would increase by approximately 5 percent if $\kappa/\lambda$ was increased from 0.2 to 0.385. Similarly, $\sigma'_r/s_u$ would be lower if $\kappa/\lambda$ was less than 0.2. The curves showing the results of VECONS are shown for values of $s_u/p'_o$ from 0.42 to 1.2.

Some conclusions to the parametric study are as

**TABLE 1 Results of CAMFE Analyses**

| Soil | $S_u$ (kips/ft$^2$) | Immediately After Installation | | | | | $s_u(\infty)$ (kips/ft$^2$) | After Consolidation | | | | | | |
|---|---|---|---|---|---|---|---|---|---|---|---|---|---|---|
| | | $p'/s_u$ | $\sigma'_r/s_u$ | $\sigma'_\theta/s_u$ | $\sigma'_z/s_u$ | $u_e/s_u$ | | $p'_{cons}/s_u$ | $\sigma'_{rc}/s_u$ | $\sigma'_{\theta c}/s_u$ | $\sigma'_{zc}/s_u$ | $\Delta p'/s_u$ | $\Delta p'/u_e$ | $\Delta\sigma'_{rc}/u_e$ |
| BBC1 | 0.750 | 1.53 | 2.58 | 0.47 | 1.53 | 3.88 | 1.143 | 3.62 | 4.73 | 3.04 | 3.10 | 2.10 | 0.54 | 0.55 |
| BBC8 | 0.881 | 1.79 | 3.03 | 0.55 | 1.79 | 3.28 | 1.224 | 3.84 | 5.08 | 3.17 | 3.26 | 2.05 | 0.63 | 0.63 |
| LC8 | 3.657 | 2.56 | 3.64 | 1.47 | 2.56 | 2.95 | 4.890 | 4.60 | 5.69 | 4.02 | 4.09 | 2.04 | 0.69 | 0.69 |
| UHCC | 1.436 | 2.23 | 3.33 | 1.14 | 2.24 | 3.83 | 2.218 | 4.68 | 5.83 | 4.08 | 4.13 | 2.45 | 0.64 | 0.65 |
| SFBM | 0.346 | 1.48 | 2.53 | 0.43 | 1.48 | 40.5 | 0.456 | 3.20 | 4.19 | 2.71 | 2.71 | 1.72 | 0.42 | 0.41 |
| St. Alban | 0.206 | 1.66 | 2.71 | 0.60 | 1.66 | 4.31 | 0.268 | 3.49 | 4.48 | 2.99 | 2.99 | 1.83 | 0.42 | 0.41 |

**TABLE 2 Results of VECONS Analyses**

| Soil | Immediately After Driving | | | | | After Consolidation | | | | | | |
|---|---|---|---|---|---|---|---|---|---|---|---|---|
| | $p'/s_u$ | $\sigma'_r/s_u$ | $\sigma'_\theta/s_u$ | $\sigma'_z/s_u$ | $u_e/s_u$ | $p'_{cons}/s_u$ | $\sigma'_{rc}/s_u$ | $\sigma'_{\theta c}/s_u$ | $\sigma'_{zc}/s_u$ | $\Delta p'/s_u$ | $\Delta p'/u_e$ | $\Delta\sigma'_{rc}/u_e$ |
| BBC1 | 1.61 | 2.62 | 0.62 | 1.62 | 3.73 | 2.89 | 4.12 | 2.04 | 2.50 | 1.28 | 0.34 | 0.40 |
| BBC8 | 1.62 | 2.62 | 0.62 | 1.62 | 3.49 | 2.85 | 4.08 | 1.99 | 2.47 | 1.23 | 0.35 | 0.42 |
| LC8 | 2.34 | 3.32 | 1.35 | 2.34 | 2.87 | 3.42 | 4.57 | 2.61 | 3.09 | 1.08 | 0.38 | 0.43 |
| UHCC | 2.36 | 3.36 | 1.36 | 2.36 | 3.55 | 3.59 | 4.52 | 2.73 | 3.21 | 1.23 | 0.35 | 0.33 |
| SFBM | 1.62 | 2.62 | 0.62 | 1.62 | 4.79 | 3.04 | 4.31 | 2.21 | 2.61 | 1.42 | 0.30 | 0.35 |
| St. Alban | 1.62 | 2.62 | 0.62 | 1.62 | 6.08 | 3.95 | 5.40 | 3.22 | 3.23 | 2.33 | 0.38 | 0.46 |

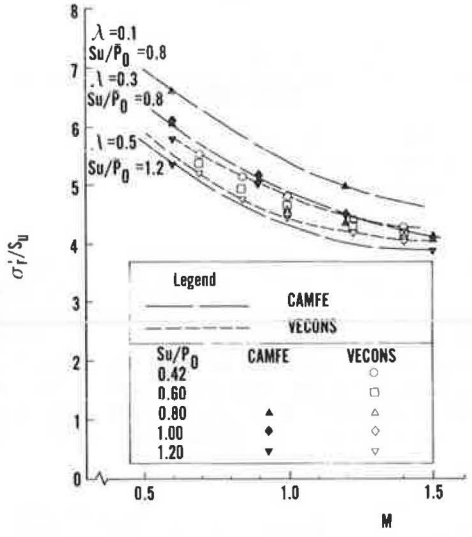


**FIGURE 3 Final radial effective stress next to pile from CAMFE VECONS.**

presented here. For both the CAMFE and the VECONS analyses, the predicted value of $\sigma'_r/s_u$ depends on the parameter M. To express the variation in quantitative terms, for $\lambda = 0.3$, $\sigma'_r/s_u$ varies from approximately 4.2 to 6.0 and for M from 1.5 to 0.6, or $\sigma'_r/s_u$ varies by 40 percent. The variation of $\sigma'_r/s_u$ with a given value of M for $\lambda$ ranging from 0.1 to 0.5 would be approximately 20 percent.

The values of $\sigma'_r/s_u$ obtained from the VECONS analyses fall in the lower one-half of the range of values obtained from the CAMFE analyses. The effect of overconsolidation, as indicated by the different ratios of $s_u/p'_o$, is minimal. This result could be expected as both analyses predict that the soil reaches the critical state during pile installation, which then infers that the soil will no longer reflect previous overconsolidation.

For the analyses, representative values of $s_u/p'_o$ were chosen as a function of OCR. The purpose of this was not only to estimate $s_u$ for the analyses but also to estimate conservative values of $s_u$ for use with Figure 3 in determining $\sigma'_{rc}$. Thus, the recommendation is to use the following table (interpolate for other values of OCR) to obtain $s_u/p'_o$, to estimate the in situ $s_u$. (Note that values of $s_u/p'_o$ greater than 1.2 are not recommended.)

| OCR | $s_u/p'_o$ |
|---|---|
| 1 | 0.42 |
| 2 | 0.60 |
| 4 | 0.80 |
| 8 | 1.0 |
| 16 | 1.2 |

## ANALYSES OF DATA

The data that were obtained in the parametric study were analyzed to derive expressions for $\sigma'_{rc}/s_u$. A linear equation results when $\sigma'_{rc}/s_u$ is expressed as a function of log M. These equations were computed by using linear regression for $\lambda = 0.3$ and $s_u/p'_o$ = 0.8, 1,0, and 1.2. The intercept values of $\sigma'_{rc}/s_u$ (the values taken at M = 1.0) were then analyzed as a function of $s_u/p'_o$, and an average value of the slopes of the linear regression lines was calculated. Equation 1, then, is the equation for $\sigma'_{rc}/s_u$ for $\lambda$ = 0.3.

$$\sigma'_{rc}/s_u = 5.15 - 0.24(s_u/p'_o) - 4.83 \log M \quad (1)$$

A similar equation that includes the variation obtained was derived for $\sigma'_{rc}/s_u$ in terms of $\lambda$, $s_u/p'_o$, and M. The data for $\lambda = 0.1$ and $\lambda = 0.5$ did not include different values of $s_u/p'_o$, so it was assumed that the variation of the regression lines ($-0.24\ s_u/p'_o$) would be the same as for $\lambda = 0.3$. The intercept values were then expressed as a linear function of $\lambda$, and the slopes of the regression lines ($\sigma'_{rc}/s_u$ versus log M) were averaged to obtain the following equation:

$$\sigma'_{rc}/s_u = 5.71 - 2.23(\lambda) - 0.24(s_u/p'_o) - 4.59 \log M \quad (2)$$

A similar approach was used to analyze the data from the VECONS analyses and a final equation was derived to represent the results for both solutions. Linear regression lines were computed for $s_u/p'_o$ =

0.42, 0.6, and 1.2. Equation 3 gives the relationship for $\sigma'_{rc}/s_u$.

$$\sigma'_{rc}/s_u = 4.91 - 0.31(s_u/p'_o) - 3.94 \log M \quad (3)$$

The final equation was derived by using a linear regression of all the data.

$$\sigma'_{rc}/s_u = 4.80 - 4.57 \log M \quad (4)$$

The correlation coefficient computed results for Equation 4 is -0.929 and the standard deviation is 0.67. Equation 1 can be used if the respective values of $\lambda$ and $s_u/p'_o$ can be estimated. The equations indicate the dependence of $\sigma'_{rc}/s_u$ on the parameters.

## ANALYSES FOR NONDISPLACEMENT PILES

Additional analyses were conducted to investigate the stress changes on piles that do not fully displace the soil. Such piles include unplugged, open-ended, pipe piles and ideal H-piles. [In some cases, soil can block off the ends of open-ended pipe piles or the sides (between the flanges) of H-piles, causing them to act as full displacement piles for further penetrations. It is not within the scope of this paper to predict whether soil would block off a pile and, if so, the depth where the soil plug would form.] For H-piles, it would be necessary to assume a circular cross-section with the same area as the H-pile as an approximation.

Analyses were conducted for partial displacement piles with displacement ratios of 0.05, 0.10, and 0.20. The displacement ratio is defined as the ratio of the cross-sectional area of steel of the piles to the gross cross-sectional area. Both of the computer solutions were programmed so that nondisplacement piles could be analyzed. According to the solutions, the soil reaches the critical state; consequently, stress changes during installation are the same as displacement piles except that the pore pressure is not as large. The critical state zone, the zone of soil at the critical state, is not as large for a nondisplacement pile.

To analyze the effects of nondisplacement piles quantitatively, a number of the cases that were used in the previous parametric study were analyzed using different displacement ratios. Based on the results of the analyses, it was concluded that the reductions in $\sigma'_{rc}/s_u$ for a displacement pile can be expressed in terms of the displacement ratio independent of M or $s_u/p'_o$. The reduction in $\sigma'_{rc}/s_u$, is expressed in terms of the value obtained for a full displacement pile. The recommendation is to reduce $\sigma'_{rc}/s_u$ computed for full displacement piles by multiplying by factors of 0.80, 0.85, and 0.90, respectively, for displacement ratios equal to 0.05, 0.10, and 0.20, respectively.

## PREDICTION OF ULTIMATE SIDE FRICTION

For rapid pile loading, undrained conditions with no soil consolidation are assumed. For undrained loading, excess pore pressure can be generated, causing changes in the effective stresses. The excess pore pressures are a fraction of the shear stresses in the soil that are caused by pile loading (3). There are also some changes in the soil stresses as a result of applied shear stress. The orientation of the major principal stress rotates around from the radial direction toward the vertical direction. To determine the state of stress at failure, it is necessary to determine both the effective stress changes caused by pile loading and the reorientation of the principal stress directions.

The results of finite element analyses on piles in clay (5) indicate that the total radial stress (excluding the hydrostatic pore pressure) acting on piles remains nearly constant during pile loading. The total radial stress at pile failure is approximately 2 to 4 percent greater than the total radial stress after consolidation except for soil near the ground surface and near the pile tip. The total radial stress increases by as much as 20 percent within approximately 5 pile radii of the ground surface. The total radial stress decreases near the pile tip. Thus, the effective radial stress after consolidation, equivalent to the total radial stress, can be used to predict the side friction capacity for the major part of the pile shaft.

The authors recommend computing the side friction capacity by using the effective radial stress after consolidation $\sigma'_{rc}$, and a friction parameter. The friction parameter is the peak total friction angle between the pile and soil, $\phi_{ss}$. Equation 5 can then be used to compute the side friction, $f_s$ as follows:

$$f_s = \sigma'_{rc} \tan \phi_{ss} \quad (5)$$

The determination of $\phi_{ss}$ can be made from undrained direct shear, direct simple shear, or rod shear tests.

The findings from two rod shear testing programs are used to estimate the friction parameter (15,16). The results that are presented here are in terms of the peak interface friction, $f_s$, and the initial effective confining (radial) pressure, $\sigma'_{ci}$. Figure 4 (16) shows a plot of $f_s$ versus $\sigma'_{ci}$ showing computed friction angles, tan $\phi_{ss} = (f_s/\sigma'_{ci})$. The range of

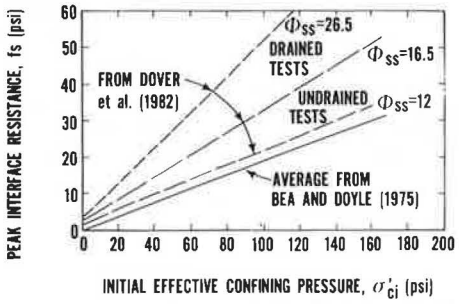


FIGURE 4 Peak interface resistance versus initial effective confining pressure *(16)*.

values of $\phi_{ss}$ for the undrained tests was from 12 to 16.5. Figure 5 (16) shows the relationship between $f_s/\sigma'_{ci}$ and the plasticity index. Ratios of $f_s/\sigma'_{ci}$ between 0.2 and 0.3, or $\phi_{ss}$ between 11 and 16 are recommended. The major conclusion from the two investigations is that there is no limit to the side friction that can be obtained. This is in contrast to the concept of limiting side friction used by the American Petroleum Institute (23).

The procedure to compute the ultimate side friction capacity is complete. Any one of Equations 1 through 4 can be used to estimate $\sigma'_{rc}/s_u$. The effective radial stress after consolidation is equivalent to $\sigma'_{ci}$ that was obtained in the laboratory rod shear tests. The ultimate side friction is computed at a number of depths using either Figure 4 or 5 to estimate $\phi_{ss}$ and Equation 5. (Some computation examples are presented later in this paper.)

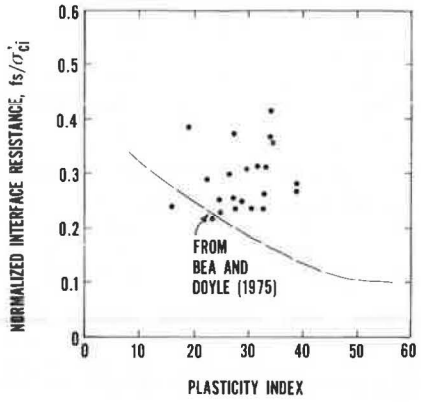


FIGURE 5 Normalized resistance versus plasticity index *(16)*.

## SOIL SOFTENING EFFECTS

Soil softening occurs in many clays after the peak side resistance is attained. A noticeable reduction in side resistance can be observed after the peak side friction occurs. The problem with designing for pile capacity is that the peak side resistance is reached in soil near the pile top and the pile tip before the ultimate pile load is applied so the maximum side resistance does not occur simultaneously along the entire length of the pile. Therefore, it is necessary to account for pile softening effects.

An evaluation of the effects of soil softening by Kraft et al. (8) is tentatively recommended. The average unit side resistance at pile failure, $f_{av}$, can be estimated by using Figure 6 (8). According to the figure, the mobilized resistance at failure depends on the pile length (L), diameter (D), stiffness (AE), and on the average maximum unit side resistance of the soil ($f_{max}$) and three other parameters. The variable u* is the relative pile-soil movement at $f_{max}$, $\mu$ is a number defining the rate that $f_s$ is decreased, and $\xi$ is a factor expressing the reduction in $f_{max}$. The variables u*, $\mu$, and $\xi$ are estimated averages for the pile length or the values at the midpoint of the pile. The curves that are shown were obtained from finite element analyses of isotropic, homogeneous soils. According to the investigators, the reduction in capacity is not sensitive to $f_{max}$ and u*.

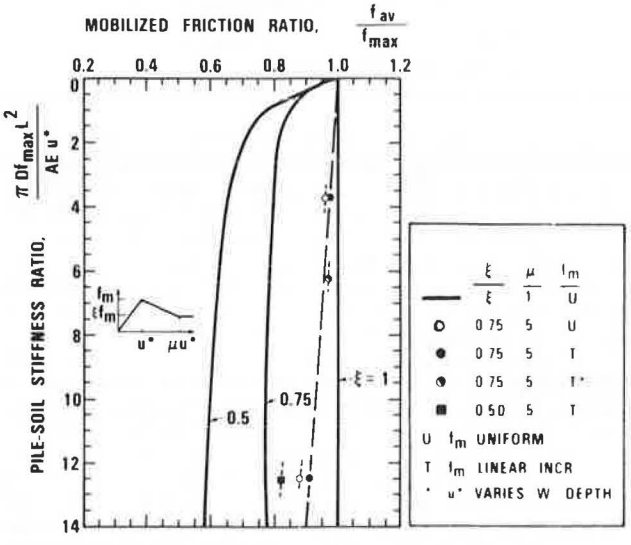


FIGURE 6 Mobilized friction ratio for soil-softening effects *(8)*.

## COMPUTATION OF PILE CAPACITY

The following equations can be used to compute the pile capacity. The side capacity, $Q_s$, can be computed by using Equation 6 assuming that there is no strain softening. To determine $Q_s$ for piles with strain-softening effects, multiply the ratio $f_{av}/f_{max}$ determined from Figure 6 by Equation 6.

$$Q_s = \left( \sum_{i=1}^{n} f_s \, \Delta L_i \right) \pi \, D \tag{6}$$

The tip capacity is computed for cylindrical piles according to Equation 7 using $N_c = 9$ and $s_u$ at the pile tip.

$$Q_p = s_u \, N_c \, \pi \, D^2/4 \tag{7}$$

(Note that the pile capacity $Q_{ult}$ is the sum of $Q_s$ and $Q_p$.)

## CONCLUSIONS AND RECOMMENDATIONS FOR USE

The parametric studies required a large number of analyses leading to the following conclusions that are true for both the CAMFE and VECONS analyses:

1. The ratio $\sigma'_{rc}/s_u$ is not dependent on $E_u$ (or G) and the in situ stress (depth).
2. The ratio $\sigma'_{rc}/s_u$, to a lesser extent, depends on the OCR, characterized by representative values of $s_u/p'_o$. (An explanation for this is that the soil is remolded during installation, removing the effects of overconsolidation.)
3. The variable $\sigma'_{rc}/s_u$ is highly dependent on the parameter M (or $\phi$).
4. Computed values of $\sigma'_{rc}/s_u$ are generally higher for the CAMFE solution.

Specific conclusions regarding the predictive procedure are as follows:

1. It is necessary to make a conservative estimate of $s_u$. The value of $s_u$ should not exceed the $s_u$ value obtained by using the table previously discussed. (See "Parametric Study of CAMFE and VECONS" elsewhere in this paper.) Normally, there is a large amount of data scatter as well as significant differences in predicted values of $s_u$, depending on the type of test that is used.
2. M should be computed using $M = 6 \sin \phi'/(3-\sin \phi')$.
3. Equations 1 through 4 should be used to determine $\sigma'_{rc}/s_u$.
4. The friction parameter $\phi_{ss}$ is probably between 11 and 16. The higher values correspond to soils with low plasticity indices. Ultimate capacities are computed using Equations 5 through 7.

## NEED FOR RESEARCH

There is a need for further research. It is difficult to determine appropriate values of $s_u$. The research should be directed at determining appropriate test procedures, either laboratory or in situ, that can be used. Correlations between soil properties (liquid limit, plasticity index, or liquidity index) and $\phi'$ would be useful and further studies on the friction parameter, $\sigma_{ss}$, are necessary. It is

probable that other solutions for the effects of pile installation will be developed, and, when this happens, similar studies should be conducted. More full-scale field tests on piles are necessary, however, to verify any predictive procedure. Design charts for different soil and pile conditions could be developed using the predictive procedure.

The recommended predictive procedure was compared to the findings of other investigations and field test data. There are some conditions that the recommended procedure has not verified experimentally. The validity of the solutions for permeable piles (concrete or timber) is questioned. The pile-soil adhesion is higher for timber piles. For nondisplacement piles (open-ended pile or H-piles), the solutions have not been verified. The strain-softening effects need to be investigated further. The solutions may not be valid for tapered (straight-sided or step-tapered) piles. The predictive procedure was developed from analytical solutions and load tests on single piles. It would not apply to piles in groups where the group effects of pile installation and loading would be significant.

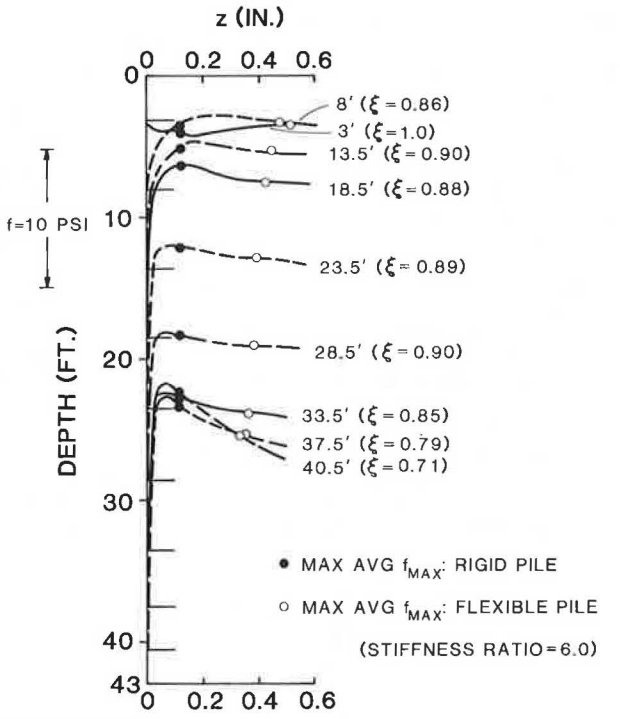


FIGURE 7 Set of f-z curves.

# Discussion

Michael W. O'Neill*

The authors describe a method to reduce average shaft resistance for flexible piles. They speculate that strain softening occurs in clay soils following the development of peak shaft resistance in driven piles. This phenomenon purportedly explains the well-known effect that average unit shaft resistance along a pile at plunging decreases with increasing pile length in relatively uniform soils. Because progressive failure occurs along the shaft, the average unit shaft resistance at plunging failure consists of contributions of peak resistances at some levels (presumably at lower levels) and post-peak (reduced) resistances at other (higher) levels. The more flexible the pile, the larger would be the post-peak reduction in unit shaft friction along the upper part of the pile; consequently, the smaller would be the average unit shaft resistance.

This writer would like to offer an alternative explanation of this phenomenon, based on full-scale and model tests that he has conducted on driven piles in clay.

Figure 7 shows a set of f-z curves for a 10.75-in.-outer diameter x 0.365-in.-wall, steel pipe pile driven to a depth of 43 ft in stiff, saturated, fairly uniform, overconsolidated clay with an OCR between 4 and 8 (24,25). Strain softening is observed to be almost nonexistent in the upper one-half of the pile but to increase markedly with depth. In the notation of the authors' Figure 6, $\xi$ at a displacement of $\mu u^* = 0.6$ in. (3 to 10 times the displacement at yield), is shown in parentheses for each level. The test pile was moderately rigid. Had it been perfectly rigid, the conditions producing the largest average side resistance, $f_{max}$, are shown by the solid dots. The value of this average $f_{max}$ is 8.97 psi.

Had the pile been much more flexible (wall thickness of 0.25 in. corresponding to a stiffness ratio of 6, using the definition in Figure 6), the average $f_{max}$ corresponding to a tip deflection of 3 percent of the pile diameter (top deflection of 5 percent of the pile diameter), which would result in plunging failure of the pile, would be derived from the points represented by the open circles. The value of the resulting average $f_{max}$ for such a flexible pile is 8.41 psi, or 6.2 percent less than the value for the rigid pile. Although the effect of pile-soil flexibility is demonstrable in this soil, it is not as significant in reducing average maximum load transfer as at least one other phenomenon, discussed below.

The results of Figure 7 have been replotted in Figure 8 in the form of $\xi$ (at 0.6 in.) versus $\Delta$, the normalized vertical distance between the pile tip and a generic depth in the soil. The variable $\xi$ is approximately constant at 0.90-0.95 for $\Delta$ exceeding 15 diameters. For $\Delta$ less than 15 diameters, $\xi$ decreases sharply to approximately 0.70 at $\Delta = 2$ diameters. This behavior suggests that the farther the pile travels past a given depth of soil during installation, the greater the degree of soil destructuring at the pile-soil interface and the higher the value of $\xi$. If such is the case, the average $f_{max}$ decreases with increasing pile penetration because the angle of soil-to-pile friction $\phi_{ss}$ decreases at a given depth as the penetration increases, assuming the correctness of the

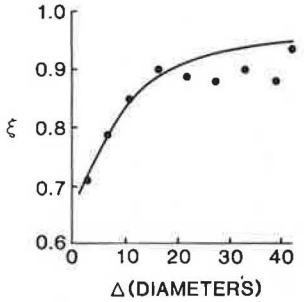


FIGURE 8 $\xi$ versus $\Delta$ for field test.

*University of Houston, Houston, Texas 77004.

assertion of the authors that lateral effective stress is generally independent of depth in a uniform soil. (The friction angle may only appear to decrease if lateral movements during driving, not accounted for by existing effective stress methods, produce permanent strain in the soil.)

If $\phi_{ss}$ decreases at a given soil depth with increasing pile penetration, the average value of $f_{max}$ should reduce in any given pile in uniform soil as it is driven deeper, even if the soil does not possess strain-softening characteristics. Figure 9 shows the results of model tests on an instrumented 1-in.-diameter, steel pipe pile driven in saturated, uniform medium-still, nonstrain-softening, low-plasticity clay (26). When the pile penetration increases from 40 diameters to, say, 80 diameters, the average $f_{max}$ decreases by 32 percent, primarily because of severe reductions in local $f_{max}$ at soil depths above 45-pile diameters with increasing tip penetration. The degree of average load transfer reduction resulting from this phenomenen (32 percent) is significant compared to the reduction caused by pile flexibility (6.2 percent in the case described).

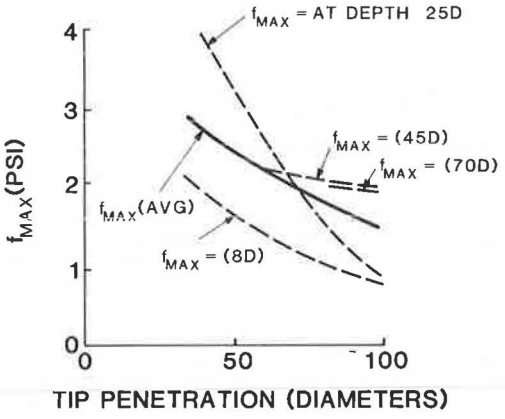


FIGURE 9 Maximum load transfer versus tip penetration for model test.

It is hoped that future theoretical effective stress studies by the authors or by others will address this issue.

REFERENCES

1. F. Baguelin, R. Frank, and J.F. Jezequel. Parameters for Friction Piles in Marine Soils. Proc., 2nd International Conference on Numerical Methods in Offshore Piling, Austin, Tex., April 1982.
2. J.P. Carter, M.F. Randolph, and C.P. Wroth. Stress and Pore Pressure Changes in Clay During and After the Expansion of a Cylindrical Cavity. International Journal for Numerical and Analytical Methods in Geomechanics. Vol. 3, 1979, pp. 305-322.
3. M.I. Esrig and R.C. Kirby. Advances in General Effective Stress Method for the Prediction of Axial Capacity for Driven Piles in Clay. Proc., 11th Offshore Technology Conference, Houston, Tex., Vol. 1, 1979, pp. 437-448.
4. J.A. Focht, Jr. and L.M. Kraft, Jr. Prediction of Capacity of Long Piles in Clay: A Status Report. Proc., Symposium on Geotechnical Aspects of Offshore and Nearshore Structures, Bangkok, Thailand, Dec. 1981.
5. A.G. Heydinger. Analysis of Axial Single Pile-Soil Interaction in Clay. Ph.D. dissertation. The University of Houston, Texas, Dec. 1982.
6. M. Kavvadas and M.M. Baligh. Non-Linear Consolidation Analyses Around Pile Shafts. Proc., 3rd International Conference on the Behavior of Offshore Structures. Vol. 2, Cambridge, Mass., Aug. 1982, pp. 338-347.
7. R.C. Kirby and M.I. Esrig. Further Development of a General Effective Stress Method for Prediction of Axial Capacity for Driven Piles in Clay. Proc., Conference on Recent Development in the Design and Construction of Piles, Institution of Civil Engineers, London, England, 1979.
8. L.M. Kraft, Jr., J.A. Focht, Jr., and S.F. Amerisinghe. Friction Capacity of Piles Driven into Clay. Journal of the Geotechnical Engineering Division. ASCE, Vol. 107, No. GT11, Nov. 1981, pp. 1521-1541.
9. T.W. Miller, J.D. Murff, L.M. Kraft, Jr. Critical State Soil Mechanics Model of Soil Consolidation Stresses Around a Driven Pile. Proc., 10th Offshore Technology Conference, Houston, Texas, Vol. 13, 1978, pp. 2237-2242.
10. M.F. Randolph, J.P. Carter, and C.P. Wroth. Driven Piles in Clay--The Effects of Installation and Subsequent Consolidation. Geotechnique. Vol. 29, No. 4, 1979, pp. 301-327.
11. C.P. Wroth, J.P. Carter, and M.F. Randolph. Stress Changes Around a Pile Driven into Cohesive Soil. Proc., Conference on Recent Developments in the Design and Construction of Piles, the Institution of Civil Engineers, London, England, 1979, pp. 163-182.
12. J.P. Carter. CAMFE, A Computer Program for the Analysis of a Cylindrical Cavity Expansion in Soil. Department of Engineering, University of Cambridge, England.
13. A.S. Vesic. Expansion of Cavities in Infinite Soil Mass. Journal of the Soil Mechanics and Foundation Division. ASCE, Vol. 98, 1972, pp. 265-290.
14. S.A. Leifer, R.C. Kirby, and M.I. Esrig. Effects of Radial Variation of Material Properties on Stress Changes Due to Consolidation Around a Driven Pile. Proc., Conference on Numerical Methods in Offshore Piling, Institution of Civil Engineers, London, England, 1979, pp. 129-135.
15. R.G. Bea and E.H. Doyle. Parameters Affecting Axial Capacity of Piles in Clay. Proc., 7th Offshore Technology Conference, Houston, Texas, Vol. 2, 1975.
16. A.R. Dover, S.R. Bamford, and L.F. Suarez. Rod Shear Interface Friction Tests in Sands, Silts, and Clays. Proc., 3rd International Conference on the Behavior of Off-Shore Structures, Cambridge, Mass., 1982.
17. R.C. Kirby and C.P. Wroth. Application of Critical State Soil Mechanics to the Prediction of Axial Capacity for Driven Piles. Proc., 9th Offshore Technology Conference, Houston, Texas, Vol. 3, 1977, pp. 483-494.
18. J.L. Withiam and F.H. Kulhawy. Analytical Modeling of the Uplift Behavior of Drilled Shaft Foundations. Contract Report B-49-3 to Niagara Mohawk Power Corporation. School of Civil and Environmental Engineering, Cornell University, Ithaca, New York, March 1978.
19. M.W. O'Neill, R.A. Hawkins, and L.J. Mahar. Field Study of Pile Group Action. Office of Research and Development, FHWA, U.S. Department of Transportation, Oct. 1982 (includes Appendixes A through F).
20. R.C. Kirby and G. Roussel. Report on ESACC

Project Field Model Pile Load Test, Hamilton Air Force Base Test Site, Novato, California. Prepared for Amoco Production Company by Woodward-Clyde Consultants, Clifton, N.J., 1980.
21. J.M. Konrad. Contribution Au Calcul de Frottement Lateral des Pieux Flottants Fonces dans des Argiles Molles et Sensibles. M.S. thesis. The Graduate School of the University of Laval, Quebec, Canada, 1977.
22. M. Roy, R. Blanchet, F. Tavenas, and P. LaRochelle. Behavior of a Sensitive Clay During Pile Driving. Canadian Geotechnical Journal. Vol. 18, July 1981, pp. 67-85.
23. American Petroleum Institute. Recommended Practice for Planning, Designing, and Constructing Offshore Platforms. API RP 2A. 9th ed., Washington, D.C., 1978.
24. M.W. O'Neill, R.A. Hawkins, and L.J. Mahar. Field Study of Pile Group Action, Appendix D. FHWA RD-81-006. FHWA, U.S. Department of Transportation, March 1981, pp. D14-D17.
25. L.J. Mahar and M.W. O'Neill. Geotechnical Characterization of Desiccated Clay. Journal of Geotechnical Engineering. ASCE, Vol. 109, No. 1, Jan. 1983, pp. 56-71.
26. R.P. Aurora, E.H. Peterson, and M.W. O'Neill. Model Study of Load Transfer in Slender Pile. Journal of the Geotechnical Engineering Division. ASCE, Vol. 106, Aug. 1980, pp. 941-945.

Publication of this paper sponsored by Committee on Foundations of Bridges and Other Structures.

*Abridgment*

# Large Observation Borings in Subsurface Investigation Programs

GAY D. JONES

ABSTRACT

The West Papago/I-10 Inner Loop Freeway alignment in Phoenix, Arizona is underlain by up to ±20 ft of surficial silty clay, sandy clay, clayey sand overburden, and ±200 ft of dense sand-gravel-cobbles (S-G-C) with occasional ±18-in boulders. Conventional, small-diameter borings are used for disturbed and undisturbed sampling in the overburden. Atterberg Limits, mechanical analyses, consolidation, collapse-potential, direct shear, and triaxial compression tests are performed on the overburden material. Refusal to helical-auger penetration usually occurs at or near the top of the S-G-C deposit. Local practice is to utilize percussion drilling to penetrate the S-G-C deposit. This procedure does not produce representative specimens of the foundation material and laboratory testing is not attempted. This paper contains a description of the composition of the subsurface materials, current drilling-sampling techniques for the S-G-C deposit, and the use of large observation borings as a supplementary means for conducting visual examination of the S-G-C material. This examination aids in the assessment of the S-G-C material as a foundation material for bridges and retaining walls, as a tunneling medium, and in the slopes of a depressed roadway.

The final link of Interstate 10 (I-10) is under design and construction by the Arizona Department of Transportation. This ±9 mi segment of the West Papago/I-10 Inner-Loop Freeway through downtown Phoenix will involve major multi-level interchanges, a depressed I-10 roadway in highly developed areas with multi-level buildings, and historic properties immediately adjacent to the alignment. The depressed roadway will intercept the surface drainage of the Phoenix Basin and separate the watershed into two regions. Storm runoff collected from the northern half of the drainage area must be conveyed through tunnels to its natural outlet at the Salt River. Subsoils through which the tunnels must be driven, and that will support structure foundations and form the depressed section side slopes, have been extensively investigated. The primary exploration method has been conventional, small-diameter drill holes with limited in-hole testing and, where feasible, acquisition of samples for use in laboratory testing.

The variation of particle sizes from clay to boulders, and material desiccation and cementation, prevents acquisition of samples suitable for laboratory testing. The absence of suitable test informa-